Published in final edited form as:
J Neurosci Res. 2011 February ; 89(2): 183–198. doi:10.1002/jnr.22542.

Insulin-Like Growth Factor-I–Forkhead Box O Transcription Factor 3a Counteracts High Glucose/Tumor Necrosis Factor-α-Mediated Neuronal Damage: Implications for Human Immunodeficiency Virus Encephalitis

Anna Wilk[1], **Katarzyna Urbanska**[2], **Shuo Yang**[3], **Jin Ying Wang**[4], **Shohreh Amini**[4], **Luis Del Valle**[1], **Francesca Peruzzi**[1], **Leonard Meggs**[1,5], and **Krzysztof Reiss**[1,*]

[1]Neurological Cancer Research, Stanley S. Scott Cancer Center, LSU Health Sciences Center, New Orleans, Louisianna

[2]Department of Genetics, University of Pennsylvania School of Medicine, Philadelphia, Pennsylvania

[3]Division of Hematology and Oncology, Northwestern University, Chicago, Illinois

[4]Department of Neuroscience, Center for Neurovirology, Temple University School of Medicine, Philadelphia, Pennsylvania

[5]Department of Nephrology, Ochsner Medical Center, New Orleans, Louisianna

Abstract

In HIV patients, antiretroviral medications trigger metabolic abnormalities, including insulin resistance. In addition, the inflammatory cytokine tumor necrosis factor-α (TNFα), which is elevated in human immunodeficiency virus encephalitis (HIVE), also induces insulin resistance and inflicts neuronal damage in vitro. In differentiated PC12 cells and rat cortical neurons, high glucose (HG; 25 mM) triggers reactive oxygen species (ROS) accumulation, contributing to the retraction of neuronal processes, with only a minimal involvement of neuronal apoptosis. In the presence of TNFα, HG-treated neurons undergo massive apoptosis. Because mammalian homolog of the Forkhead family of transcription factors, Forkhead box O transcription factor 3a (FOXO3a), controls ROS metabolism, we asked whether FOXO3a could affect the fate of differentiated neurons in the paradigm of HIVE. We observed FOXO3a nuclear translocation in HG-treated neuronal cultures, accompanied by partial loss of mitochondrial potential and gradual retraction of neuronal processes. Addition of TNFα to HG-treated neurons increased expression of the FOXO-dependent proapoptotic gene Bim, which resulted in extensive apoptotic death. Insulin-like growth factor-I (IGF-I) significantly lowered intracellular ROS, which was accompanied by IGF-I-mediated FOXO3a nuclear export and decrease in its transcriptional activity. The clinical relevance of these findings is supported by detection of nuclear FOXO3a in TUNEL-positive cortical neurons from HIVE, especially in brain areas characterized by elevated TNFα.

Keywords

IGF-I; FOXO3a; ROS; neuronal apoptosis; HIV encephalitis

*Correspondence to: Krzysztof Reiss, Neurological Cancer Research, Stanley S. Scott Cancer Center, Department of Medicine, LSU Health Sciences Center, 533 Bolivar Str. CSRB, room 526, New Orleans, LA 70112. kreiss@lsuhsc.edu.
Anna Wilk, Katarzyna Urbanska, Shuo Yang, Luis Del Valle, Francesca Peruzzi, and Krzysztof Reiss were previously with the Department of Neuroscience, Center for Neurovirology, Temple University School of Medicine, Philadelphia, Pennsylvania.

Among human immunodeficiency virus (HIV)-infected individuals, viral load and the use of highly active antiretroviral therapy (HAART) have been linked with the development of severe metabolic abnormalities (Chandra et al., 2009; Krause et al., 2009; Rosso and Di Biagio, 2009; Vigano et al., 2009). Studies conducted before the widespread use of HAART indicate that HIV infection is associated with increased blood levels of triglycerides and the presence of small, dense low-density lipoprotein (LDL) particles (Grunfeld et al., 1989; Feingold et al., 1993; Shor-Posner et al., 1993). The addition of antiretroviral medications, in particular, the use of protease inhibitors, often leads to the development of insulin resistance and type 2 diabetes mellitus in this already susceptible population (Walli et al., 1998; Carr et al., 1999; Calza et al., 2003; Nishikawa et al., 2003). Importantly, this severe deregulation of glucose metabolism is closely associated with the development of cerebrovascular disease, neuronal damage, and an elevated rate of dementia (Valcour et al., 2004a, 2005, 2006; Hadigan, 2005, 2006; Salehian et al., 2005; Koeppe and Kosmiski, 2006; Valcour and Paul, 2006).

Hyperglycemia is associated with an exponential increase in the accumulation of reactive oxygen species (ROS; Nishikawa et al., 2000; Kang et al., 2003b), which contribute to multiorgan diabetic complications, including the CNS (Ting et al., 1996; Baynes and Thorpe, 1999). ROS-mediated damage has also been linked to defects in genomic maintenance and accelerated aging (Hasty et al., 2003). We have shown recently a strong antioxidant action of insulin-like growth factor-I receptor (IGF-IR) in mesangial cells maintained at high glucose concentration (Kang et al., 2003b; Chintapalli et al., 2007). This novel anti-ROS effect of the IGF-IR was closely coupled with the improvement of mesangial cell survival and increased involvement of homologous recombination directed repair of DNA double strand breaks (Yang et al., 2005) and suggested the contribution of IGF-I–Forkhead box O transcription factor 3a (FOXO3a) signaling axis in preventing HG-mediated ROS accumulation (Zheng et al., 2000; Chintapalli et al., 2007; Essaghir et al., 2009). FOXO3a modulates expression of genes involved in a wide variety of cellular processes, including apoptosis, cell cycle arrest, responses to DNA damage, oxidative stress, and glucose metabolism (Burgering and Kops, 2002). It undergoes inhibitory phosphorylation by signaling kinases such as Akt, SGK, and CDK2, which results in cytoplasmic sequestration of FOXO3a via its direct binding to 14-3-3 (Chong and Maiese, 2007). In contrast, stress-related signaling molecules such as JNK, MST1, and tumor necrosis factor-α (TNFα) have been shown to activate FOXO3a transcriptional activity (Lee et al., 2008). Indeed, stress associated with serum starvation or ROS accumulation can trigger FOXO3a nuclear translocation and its elevated transcriptional activity (Chintapalli et al., 2007; Hasegawa et al., 2008; Nakamura and Sakamoto, 2008). Therefore, one could postulate that FOXO3a has the potential of controlling the fate of cells in response to stress and the availability of survival factors. This could be achieved by modulating the expression of genes that may control contradictory functions within the affected cell. For example, FOXO3a transcriptional activity could direct affected cells to apoptosis via expression of proapoptotic genes such as Bim, FAS ligand, or TRAIL (Gilley et al., 2003; Nakamura and Sakamoto, 2008). On the other hand, the same FOXO3a may increase cell survival by transcriptional activation of cell cycle inhibitors ($p27^{kip1}$, $p21^{waf1}$) or by inhibition of cyclin D1 and D2 (Lees et al., 2008; Rathbone et al., 2008; Burhans and Heintz, 2009), which in turn could gain necessary time for oxidative detoxification via activation of MnSOD and catalase expression (Kops et al., 2002; Choi et al., 2009) or for DNA repair via activation of Gadd45 (Zheng et al., 2005).

Our current study shows that a 25 mM glucose concentration applied for 16 hr (referred to here as high glucose; HG) elevated accumulation of ROS in differentiated PC12 neuron-like cells and in primary cultures of rat cortical neurons (RCN). IGF-I decreased ROS

accumulation and enhanced stability of neuronal processes in long-term (8–10 days) cultures exposed to HG. The observed accumulation of ROS in the presence of HG was accompanied by translocation of FOXO3a to the nucleus, loss of mitochondrial potential, and slow but continuous retraction of neuronal processes, which happened with only minimal involvement of neuronal apoptosis. Importantly, more severe and possibly permanent neuronal damage was observed when HG-treated neuronal cultures were exposed to TNFα. This detrimental action of HGα TNFα shifted FOXO3a nuclear activity toward the expression of the FOXO-dependent proapoptotic protein Bim and triggered neuronal apoptosis, which was partially prevented by IGF-I. The clinical relevance of these in vitro findings was supported by a strong nuclear presence of FOXO3a in TUNEL-positive cortical neurons from HIV encephalitis (HIVE), which was found preferentially in the brain areas characterized by elevated TNFα.

MATERIALS AND METHODS

Cell Culture

Detailed culture conditions for proliferation and differentiation of PC12 rat pheochromocytoma neuron-like cells (ATCC CRL-1721) are described in our previous publications (Ying Wang et al., 2003; Wang et al., 2006, 2007). To emphasize the effects of IGF-I stimulation on neuronal survival, we have utilized PC12/GR15 cells previously generated in our laboratory, which in addition to endogenous rat IGFIR gene overexpress human IGF-IR cDNA (Ying Wang et al., 2003). To induce neuronal differentiation, PC12/GR15 cells were plated on collagen IV (Sigma, St. Louis, MO)-coated dishes and treated with 20 ng/ml NGF (Invitrogen, Carlsbad, CA) in the absence of serum. Neuronal processes began to form within the first 24 hr following the treatment and could be preserved as fully differentiated neuronal processes for at least 2 weeks. For ROS measurements, PC12/ GR15 cells were allowed to differentiate in the presence of NGF for 5 days. The medium was changed to fresh serum-free medium (SFM) containing either normal glucose concentration (5 mM; NG) or high glucose concentration (25 mM; HG). In some experiments, the cells were treated with IGF-I (50 ng/ml; Invitrogen) and/or with TNFα as previously described (Ying Wang et al., 2003; Wang et al., 2006).

Primary Cultures of Rat Cortical Neurons

The cells were obtained by enzymatic and mechanical extraction from Sprague Dawley rat embryos (embryonic day 17; Aprea et al., 2006). Brains were removed under a preparative microscope in dissecting medium (1.6 mM sucrose, 2.2 mM glucose, 1 mM Hepes, 16 mM NaCl, 0.5 mM KCl, 0.1 mM Na_2HPO_4, and 0.022 mM KH_2PO_4) and placed in Hybernate E medium (BrainBits, Springfield, IL). After careful removal of the meninges, the intact brain tissue was incubated with TripleExpress enzyme (Gibco, Invitrogen, Carlsbad, CA) at 37°C for 10 min, followed by three washes with Hybernate E medium (Aprea et al., 2006). Tissue trituration was performed in culture medium (see below) using a fire-polished glass Pasteur pipette, and single-cell suspension was resuspended in Neurobasal medium containing B27 supplement, 0.25 mM glutamax, and 0.25 mM L-glutamine (all from Gibco, Invitrogen). The cells were plated on poly-D-lysine-coated dishes at a density of $4.5 \times 10^4/cm^2$.

ROS Measurements

The methodology described in our previous work was followed, with minor modifications (Yang et al., 2005; Chintapalli et al., 2007). The cells were preloaded with 1 μM oxidant-sensitive dye redox sensor red CC-1 and with 50 nM of mitochondrial specific dye MitoTracker green FM. Intracellular ROS was visualized under an inverted Nikon Eclipse TE300 microscope equipped with a Retiga 1300 camera, motorized z-axis, and deconvolution software (SlideBook4; Intelligent Imaging Innovations, Denver, CO).

The kinetics of ROS metabolism at NG (5 mM) and HG (25 mM) was determined by measuring the intensity of fluorescent signal from the redox-sensitive fluoroprobe 2′,7′-dichlorofluorescein diacetate (DCFDA) at multiple time points. DCFDA is converted by intracellular esterases to 2′,7′-dichlorodihydrofluorescein, which in turn is oxidized by H_2O_2 to highly fluorescent 2′,7′-dichlorohydrofluorescein (DCF). Briefly, differentiated PC12 were loaded with 10 μM DCFDA in phenol red-free DMEM containing either 5 mM or 25 mM glucose. Cells were incubated in a 24-well plate at 37°C for 30 min and washed with phenol red-free DMEM. DCF fluorescence was detected by a Fluorescence Multi-Well Plate Reader CytoFluor 4000 set for excitation 485 nm and emission 530 nm (PerSeptive Biosystems). The intensity of fluorescent signal proportional to the accumulated ROS at different time points following HG, and in the presence or absence of IGF-I stimulation, was calculated according to the equation described originally by Wang and Joseph (1999) and in our previous work (Chintapalli et al., 2007).

Mitochondrial Membrane Potential

We used a flow cytometry-based MitoPotential Kit according to the manufacturer's protocol (Guava EasyCyte). Loss of the mitochondrial inner transmembrane potential ($\Delta\psi m$) was measured by a cationic dye, JC-1, which gives either green or orange fluorescence depending on mitochondrial membrane depolarization. After 24 hr of incubation in HG or NG, the cells were harvested by trypsinization, loaded with JC-1 reagent for 30 min, and immediately analyzed by Guava EasyCyte flow cytometer using Mito-Potential software. Cell treatment with the ionophore valinomycin, which fully depolarizes mitochondria, was utilized as a positive control (Troiano et al., 2007).

Western Blotting

To obtain total protein extracts, PC12 cells were lysed for 5 min on ice with 400 μl lysis buffer A [50 mM HEPES, pH 7.5, 150 mM NaCl, 1.5 mM $MgCl_2$, 1 mM EGTA, 10% glycerol, 1% Triton X-100, 1 μM phenylmethylsulfonyl fluoride (PMSF), 0.2 mM Na-orthovanadate, and 10 μg/ml aprotinin]. Protein extracts (50 μg) were separated on a 4–15% gradient SDS-PAGE (Bio-Rad, Hercules, CA) and transferred to nitrocellulose membranes. Subcellular fractionation was applied to separate cytoplasmic and nuclear proteins using the Nuclear/Cytosol Fractionation kit (Thermo Scientific, Rockford, IL), with some modifications (Trojanek et al., 2003). The blots were analyzed by anti-FOXO3a rabbit polyclonal antibody (Cell Signaling Technology, Danvers, MA), and the purity of nuclear and cytosolic fractions was determined by anti-Lamin A/C rabbit polyclonal antibody and anti-α-tubulin mouse monoclonal antibody (Santa Cruz Biotechnology, Santa Cruz, CA), respectively.

FOXO3a Transcriptional Activity

The reporter plasmid contains luciferase gene driven by FOXO3a-responsive elements (FHRE), which consist of three copies of FHRE from the fragment of the human Fas ligand promoter, which was amplified and cloned into pGL3 vector (Brunet et al., 1999). PC12 cells were cotransfected with firefly-*Renilla* and FHRE-luciferase plasmid DNAs (ratio 1/3) by utilizing lipofectamine 2000 (Invitrogen). The activation of FHRE was evaluated by a dual firefly-*Renilla* luciferase reporter system (Promega, Madison, WI) by utilizing Synergy 2 luminometer and Gen 5 software (BioTech).

Immunocytofluorescence and Immunohistochemistry

Differentiated PC12 cells cultured on collagen IV-coated microscopic chambers were fixed and permeabilized with buffer containing 0.02% Triton X-100 and 4% formaldehyde in PBS. The fixed cells were washed three times in PBS and blocked in 5% BSA for 30 min at

37°C. Subcellular distribution of FOXO3a was evaluated by utilizing anti-FOXO3a rabbit polyclonal antibody (Cell Signaling), followed by FITC-conjugated goat anti-rabbit secondary antibody (Molecular Probes, Eugene, OR).

Formalin-fixed, paraffin-embedded HIVE clinical samples were sectioned at 4 μm thickness, mounted on electromagnetically charged glass slides, and stained with hematoxylin-eosin for routine histological analysis. Immunohistochemistry was performed by using the avidin-biotin-peroxidase complex system, according to the manufacturer's instructions (Vectastain Elite ABC Peroxidase Kit; Vector Laboratories, Burlingame, CA). Briefly, sections were deparaffinized in xylene and rehydrated through descending grades of alcohols up to water. For nonenzymatic antigen retrieval, the sections were heated in 0.01 M sodium citrate buffer (pH 6.0) to 95°C under vacuum for 40 min and allowed to cool for 30 min at room temperature. The slides were rinsed with PBS and incubated in MeOH/3% H_2O_2 for 20 min to quench endogenous peroxidase. Sections were then washed with PBS and blocked in PBS/0.1% BSA containing 5% normal goat or horse serum for 2 hr at room temperature. Sections were incubated overnight at room temperature with the following primary antibodies: anti-FOXO3a rabbit polyclonal (Cell Signaling), anti-TNFα mouse monoclonal (Chemicon, Temecula, CA), antisynaptobrevin mouse monoclonal (Synaptic Systems, Gottingen, Germany). Biotinylated anti-rabbit and anti-mouse secondary antibodies were used at room temperature for 1 hr. Avidin-biotin peroxidase complex steps were performed according to the manufacturer's instructions (Vector Laboratories). Finally, the sections were developed with a diaminobenzidine substrate, counterstained with hematoxylin, dehydrated through alcohols, cleared in xylene, and coverslipped with Permount.

We have utilized dual-color immunofluorescence to evaluate how subcellular localization of FOXO3a correlates with apoptosis (TUNEL positive nuclei). Specifically, rabbit anti-FOXO3a antibody was detected with rhodamine-conjugated anti-rabbit IgG, and the TUNEL-positive nuclei were detected by FITC-based fluorescent labeling according to the manufacturer's recommendations (Fluorescein In Situ Cell Death Detection Kit; Roche). The images were visualized with an inverted Nikon Eclipse TE300 microscope equipped with a Retiga 1300 camera, motorized z-axis, and deconvolution software (SlideBook4). Series of three-dimensional images of each individual picture were deconvoluted to one two-dimensional picture and resolved by adjusting the signal cutoff to near-maximal intensity to increase resolution. Nikon Plan Fluor ×100/1.3 oil, and ×40/1.3 oil objectives were utilized.

Real-Time RTPCR

Total RNA was extracted from 1.5×10^6 PC12 cells with RNAqueous kit (Ambion, Austin, TX), according to the manufacturer's protocol. Three micrograms of total RNA was denatured and reverse transcribed using oligo$(dT)_{15}$ primers and M-MLV reverse transcriptase (Invitrogen). PCRs were performed with the LightCycler 480 SYBR Green I Master (Roche) using the following primers for rat: Bim: (forward) 5′-CAGAGATACGGATCGCACAG-3′, (reverse) 5′-ACCAGACGGAAGATGAATCG-3′ (amplification product 151 bp); MnSOD: (forward) 5′-ACGCGACCTACGTGAACAATCTGA-3′, (reverse) 5′-TCCAGCAACTCTCCTTTGGGTTCT-3′(amplification product 193 bp); GAPDH: (forward) 5′-TCTACCCACGGCAAGTTCAA-3′, (reverse) 5′-GGTTTCTCCAGGCGGCATGT-3′ (amplification product 605 bp).

Quantitative analysis of cDNA amplification was assessed by incorporation of SYBR Green into double-stranded DNA. Measurement of gene expression was performed by using the LightCycler 480 Instrument (Roche) and analyzed with Relative Quantification LightCycler 480 Multiple Plate Analysis software. PCR containing 50 ng cDNA template, 0.5 μM each

of forward and reverse primers, and SYBR Green PCR Master Mix was performed in a total volume of 20 μl. The amplification conditions were initial incubation of 10 min at 95°C, followed by 45 cycles: 30 sec at 95°C; 1 min at 60°C, and 1 min at 72°C. All cDNA samples were tested in duplicate. The samples were compared by using the relative Ct method. The Ct value, which is inversely proportional to the initial template copy number, is the calculated cycle number when the fluorescence signal is significantly above background level. The -fold increase or decrease was measured relative to controls and calculated after adjusting for GAPDH using $2^{-}[\Delta\Delta Ct]$, where ΔCt = Ct Bim − Ct GAPDH and $\Delta\Delta Ct$ = ΔCt treatment − ΔCt control.

siRNA Treatment

Differentiated PC12/GR15 cells were transfected with 100 and 200 nM of “on-target plus” smart pool siRNAs against rat Bim and rat FOXO3a mRNA (Thermo Scientific) or with control siRNA against nuclear lamins (Chintapalli et al., 2007) by using Lipofectamine 2000 (Invitrogen). After 72 hr of cell exposure to siRNAs, protein extracts were prepared and tested for Bim and FOXO3a protein levels by Western blot analysis. Parallel siRNA-treated cultures were analyzed for the presence of apoptotic cells by TUNEL assay.

RESULTS

IGF-I Attenuates HG-Mediated ROS Accumulation and Prevents Retraction of Neuronal Processes

It has been reported that diabetes mellitus and associated hyperglycemia alter redox status of the cell through the accumulation of ROS by the mitochondrial electron transport chain and in cytoplasm by the action of NADPH oxidase (Kang et al., 2003a,b; Susztak et al., 2006). Our results indicate that HG (25 mM) elevated accumulation of ROS in differentiated PC12 neuronlike cells (Fig. 1) and in primary cultures of rat cortical neurons (RCN; see Fig. 3A) compared with the corresponding cultures kept under NG (5 mM). The accumulated ROS were found in neuronal processes and in perinuclear cytoplasm and were at least threefold higher than ROS levels detected in differentiated neuronal cells kept in NG culture conditions (Fig. 1B). The treatment of cells with the ROS scavenger N-acetylcysteine (NAC; 500 μM) decreased HG-mediated ROS accumulation to the background values of ROS observed in NG (Fig. 1A,B). We have previously reported that IGFI protects differentiated neurons from different proapoptotic insults (D’Ambrosio et al., 1997; Valentinis et al., 1998, 1999) and prevents TNFα-induced retraction of neuronal processes (Ying Wang et al., 2003; Wang et al., 2006). To emphasize the protective effects of IGF-IR signaling, we have previously generated PC12 cells, which, in addition to the endogenous rat IGF-IR gene, express human IGF-IR (PC12/GR15; Ying Wang et al., 2003). Our results, depicted in Figure 1B, show that IGF-I, in a manner similar to NAC, inhibited HG-induced accumulation of ROS and increased stability of neuronal processes both in HG-treated PC12/GR15 cells (Fig. 2A) and in HG-treated RCN (Fig. 3B). Interestingly, the extensive loss of neuronal processes observed in vitro following prolonged cell exposure to HG was accompanied by only a slight increase in neuronal apoptosis. In particular, under 8% of PC12/GR15 cells (Fig. 2B) and under 5% of RCN (Fig. 3C) underwent apoptotic cell death after 10 days in HG, which corresponds to the background levels of apoptotic death observed in these neuronal cultures. However, HG treatment resulted in a significant loss of mitochondrial potential detected in PC12/GR15 cells 5 days after the HG treatment, which was effectively prevented by exposing HG-treated cells to IGF-I (50 ng/ml; Fig. 2C). Importantly, IGF-I also inhibited HG-induced retraction of neuronal processes in both differentiated PC12/GR15 (Fig. 2A) and in RCN (Fig. 3A), which supports our previous observations in which IGF-I protected mouse and human mesangial cells from cellular damage induced by HG (Yang et al., 2005; Chintapalli et al., 2007). To quantify the loss of

neuronal processes, we have measured the average length of neuronal processes in randomly selected microscopic fields by utilizing Image J software, as described in our previous work (Ying Wang et al., 2003). At day 10 in NG, the average length of neuronal processes per field was 2,559 ± 253 μm, which decreased more than 6-fold in the presence of HG (394 ± 98 μm). Importantly, when the HG incubation was accompanied by IGF-I, retraction of neuronal processes was effectively prevented (2,085 ± 132 μm). Neuronal loss in primary cultures of RCN is shown in Figure 3B. In these cells, loss of neuronal processes looked different than in cultures of differentiated PC12. Instead of retraction, we observed a slow disintegration and fragmentation of the processes (Fig. 3B, middle panel). Despite this, the presence of IGF-I in HG-treated cultures of RCN improved significantly the integrity of neuronal processes in HG-treated cultures (Fig. 3B, last panel). Also, the contribution of apoptotic cell death to HG-mediated neuronal damage was minimal (Fig. 3C).

Changes in FOXO3a Subcellular Localization and Transcriptional Activity in Response to HG and IGF-I

Because ROS metabolism and IGF-I signaling have been both linked to FOXO3a function (Kops et al., 2002; Davila and Torres-Aleman, 2008; Nakamura and Sakamoto, 2008; Matheny and Adamo, 2009; De Bruyne et al., 2010), we evaluated FOXO3a subcellular localization in differentiated PC12/GR15 cells in response to HG and IGF-I stimulation. The purpose of this experiment was to determine wherther FOXO3a, which is the key transcription factor for anti-ROS enzymes [superoxide dysmutases (Mn-SOD) and catalases] and for proapoptotic proteins (Bim, FAS lignad, and PUMA; Liu et al., 2005; Dansen and Burgering, 2008), can potentially control neuronal fate in response to the stress and survival factors. Figure 4A shows digital images collected from the midsection of the nucleus of PC12/GR15 cells. In NG, FOXO3a-associated green immunofluorescence was detected preferentially in the cytoplasmic compartment of differentiated PC12/GR15 cells. Notably, we observed a dramatic shift of FOXO3a from cytoplasm to the nucleus (blue fluorescence, DAPI) during first 16 hr of cell exposure HG (PC12/HG). This nuclear translocation of FOXO3a was partially prevented when HG-treated PC12/GR15 cells were exposed either to IGFI (PC12/HG + IGF) or to the ROS scavenger NAC (PC12/HG + NAC). Quantitatively, colocalization of FOXO3a with DAPI-labeled nuclei increased from 18% in NG to 62% in HG culture conditions (Fig. 4B). This over 3-fold increase in FOXO3a nuclear content was significantly reduced when the HG-treated cells were cultured in the presence of IGF-I or NAC (Fig. 4A,B).

We have confirmed HG- and IGF-I-mediated changes in FOXO3a localization by utilizing subcellular fractionation and Western blot analysis (Fig. 4C). Although with this technique we did not observe the expected changes in levels of FOXO3a in cytosolic fractions, we observed almost a 3-fold increase in nuclear FOXO3a in the presence of HG (Fig. 4D), and this elevated fraction of nuclear FOXO3a was reduced when HG-treated PC12/GR15 were exposed to IGF-I (Fig. 4B,D). This nuclear shift of FOXO3a in HG was accompanied by increased FOXO3a transcriptional activity (Fig. 4E). Luciferase-based FOXO3a reporter assay demonstrated elevated FOXO3a transcriptional activity in the presence of HG, which decreased significantly following the treatment with IGF-I (HG + IGF-I).

Simultaneous Action of HG and TNFα Triggers Neuronal Apoptosis

We have shown previously that the inflammatory cytokine TNFα causes retraction of neuronal processes in the absence of apoptotic cell death (Wang et al., 2006), in a manner similar to the retraction of neuronal processes observed here following prolonged cell exposure to HG. In HIV encephalitis TNFα has been found elevated in the brain regions characterized by inflammation (Ryan et al., 2004; Hoffmann et al., 2009; Xing et al., 2009), and antiretroviral medications, including HAART, often lead to deregulation of glucose and

lipid metabolism (Hui, 2003; Domingos et al., 2009), so we asked how differentiated neurons will respond to the elevated concentration of glucose in the presence of TNFα. The results depicted in Figure 5A demonstrate that neither HG nor TNFα, when added separately, elevated neuronal apoptosis even if the corresponding treatments lasted up to 10 days, a condition in which retraction of neuronal processes is already apparent (Fig. 2A). However, when these two potentially detrimental factors were applied together, a strong induction of neuronal apoptosis was observed as early as 5 days following the treatment. Quantitatively, 5 days of exposure to HG + TNFα triggered apoptosis in 32.2% ± 5.1% of differentiated PC12/GR15 cells. Note that the level of neuronal apoptosis detected in NG is 7.2% ± 2%, in HG is 9.7% ± 1.9%, and in TNFα is 11.5% ± 2.8%. These changes were not statistically significant. In the presence of IGF-I or NAC, the levels of neuronal apoptosis triggered by HG + TNF declined from 32.2% to 16.1% and 14.2%, respectively ($P = 0.05$).

Next, we asked how changes in FOXO3a subcellular distribution and its elevated overall transcriptional activity correlate with specific gene expression. In particular, we evaluated mRNA levels for anti-ROS protein MnSOD and proapoptotic protein Bim (Fig. 5B). We have selected these two FOXO3a-dependent genes to evaluate whether in our experimental model FOXO3a acts to protect cells from HG-mediated cellular damage (anticipated increase in MnSOD mRNA) or might act as an activator of cell death via elevated expression of Bim. Surprisingly, results from real-time RTPCR demonstrate only small changes in the amounts of MnSOD mRNA when differentiated PC12/GR15 were exposed to HG, TNFα, or the combination of HG + TNFα for 5 days. With respect to Bim mRNA, HG treatment resulted in a 1.3-fold increase over NG (not significant), and TNFα treatment did not affect Bim mRNA levels. In contrast, Bim mRNA increased over 8-fold in PC12/ GR15 cells exposed to the combination of HG + TNFα. In the presence IGF-I, HG + TNFα stimulation of Bim expression decreased significantly, which correlated well with the improved survival of PC12/GR15 cells in the presence of IGF-I (Fig. 5A). Our results indicate that the observed peak in apoptotic death of differentiated PC12/GR15 cells happened when HG treatment was accompanied by elevated TNFα, which may depend on FOXO3a transcriptional activation of proapoptotic Bim. Next, we used siRNAs against Bim and FOXO3a to verify their involvement in triggering neuronal apoptosis in our experimental setting. Results in Figure 5C show a 3-fold reduction in Bim and a 2.2-fold reduction in FOXO3a protein levels following 72 hr exposure of PC12/GR15 cells to 200 nM of Bim and FOXO3a siRNAs, respectively. Note that irrelevant siRNA against nuclear lamins (NL) was completely ineffective at down-regulating Bim and FOXO3a. Importantly, this partial down-regulation of Bim, as well as the down-regulation of FOXO3a, resulted in a significant decrease in apoptotic cell death induced in differentiated PC12/GR15 cells by the combined treatment with HG and TNFα, further supporting the idea that FOXO3a-dependent activation of Bim expression is involved in neurotoxicity by a combined action of HG and TNFα.

Immunohistochemical Evaluation of Neuronal Damage in HIVE in Association With TNFα Accumulation and Nuclear Localization of FOXO3a

We have characterized areas of HIV encephalitis by the detection of perivascular accumulation of inflammatory cells, predominantly macrophages and lymphocytes, among which giant multinucleated cells are often observed (not shown). These cuffs of inflammatory cells are located mostly in the subcortical white matter, although their presence has been described also in the cortex (Del Valle and Pina-Oviedo, 2006). Another histological feature used in the evaluation is the presence of parenchymatous microglial nodules, which are the result of microglial cell activation, again located mostly in subcortical white matter. These prominent inflammatory changes usually result in white matter pallor and the detection of reactive astrocytes. Results in Figure 6A demonstrate the

overall experimental approach for the selection of the inflammation affected (area 2) and unaffected (area 1) regions in the brains of patients diagnosed with HIVE. Immunohistochemistry for TNFα shows practically undetectable levels of this inflammatory cytokine in area 1 and robust TNFα immunoreactivity in area 2 (Fig. 6B). We have labeled neuronal processes in consecutive sections corresponding to area 1 and area 2 by with antisynaptobrevin antibody, which shows qualitative differences in the density of neuronal processes between these two experimentally selected areas of the brain (Fig. 6B). In the next set of experiments, we evaluated subcellular distribution of FOXO3a in neurons from unaffected regions of the brain (area 1 from Fig. 6) in comparison with the regions affected by the inflammation (area 2 from Fig. 6). As shown in Figure 7A, neurons from unaffected areas are characterized by cytoplasmic FOXO3a immunolabeling in which a weak nuclear presence was detected (area 1; arrows). In contrast, most neurons found in the vicinity of ongoing inflammation showed a strong nuclear and cytoplasmic FOXO3a immunolabeling (area 2; arrows). We have also performed double labeling for FOXO3a and TUNEL (Fig. 7B). The results show that the neurons found in the affected regions of the brain (area 2) in which strong nuclear presence of FOXO3a was detected were also TUNEL positive. Importantly, over 90% of neurons characterized by strong nuclear FOXO3a immunolabeling were TUNEL positive. Further quantitative evaluations of multiple HIVE clinical samples are required to determine the magnitude of neuronal apoptosis in association with TNFα accumulation and FOXO3a nuclear translocation and to verify whether indeed ROS accumulation contributes to proapoptotic action of TNFα in vivo and whether it correlates with HIV-associated dementia.

DISCUSSION

This study demonstrates synergy between HG-mediated accumulation of ROS and the presence of TNFα in triggering neuronal apoptosis, which may contribute to the development of cognitive abnormalities observed in patients with chronic HIVE. The apoptotic loss of differentiated neurons was minimal when either TNFα (Wang et al., 2006) or HG (this paper) was introduced separately. In addition, we have shown that IGF-I treatment counteracted HG-mediated accumulation of ROS, prevented retraction of neuronal processes, and more importantly attenuated neuronal apoptosis triggered by HG + TNFα. These anti-ROS prosurvival effects of IGF-I were associated with FOXO3a nuclear export, overall decrease of FOXO3a transcriptional activity, and attenuation of FOXO3a-dependent expression of the proapoptotic protein Bim. Interestingly, similar neuroprotective effects were observed when HG + TNFα treatment was accompanied by the ROS scavenger NAC (Fig. 5A), further indicating the involvement of ROS accumulation in the observed neuronal apoptosis. In addition, we have found multiple examples of apoptotic neurons with strong FOXO3a nuclear immunolabeling in clinical samples of HIVE. These FOXO3a-positive apoptotic nuclei were detected almost exclusively in the regions of the brain in which TNFα was elevated (Figs. 6, 7). These new results are different from our previous observations in kidney mesanglial cells, in which nuclear FOXO3a was associated with improved cell survival (Chintapalli et al., 2007). The only explanation for this apparent discrepancy is that FOXO3a activity might be different depending on the type and degree of the stress and possibly might also depend on different cellular contexts. For instance, our preliminary unpublished observations with diabetic kidney indicate elevated levels of the anti-ROS protein MnSOD, whose expression can be positively regulated by FOXO3a. Note that our present results obtained from HG− + TNF-treated PC12 cells demonstrate high Bim mRNA levels in the absence of MnSOD transcriptional activation (Fig. 5B). Therefore, in this particular experimental setting, lack of MnSOD activation may be responsible for shifting FOXO3a activity toward apoptosis. For example, FOXO3a transcriptional activity can induce apoptosis via expression of proapoptotic genes such as Bim, FAS ligand, or TRAIL (Gilley et al., 2003; Nakamura and Sakamoto, 2008). On the other hand, FOXO3a may

increase cell survival by transcriptional activation of oxidative detoxification via MnSOD and catalase expression (Kops et al., 2002; Choi et al., 2009). Further experiments are required to explain why HG-induced ROS failed to increase MnSOD transcription in differentiated PC12/GR15 cells.

HG in the blood is known to increase ROS accumulation, leading to oxidative damage in different organs, including the CNS. Deregulation of glucose homeostasis has recently been considered as a serious risk factor for cognitive impairment among HIV-infected individuals (Valcour et al., 2005, 2006). This impairment of the mental status became even more important in view of recent findings that protease inhibitors, which are the major components of highly active antiretroviral therapy (HAART), may cause glucose intolerance and may lead to the development of type 2 diabetes mellitus (Valcour et al., 2005; Larson et al., 2006). Two potential mechanisms are associated with this underappreciated metabolic impairment: direct interaction between protease inhibitors and glucose transporter GLUT4 (Hertel et al., 2004) and/or interference with cellular retinoic acid binding protein type I (CRABP-I), which under normal circumstances is expected to support PPARγ-mediated down-regulation of free fatty acids and inhibition of TNFα (Barbaro, 2003, 2006). As a result, HIV-associated metabolic abnormalities, insulin resistance, and type 2 diabetes may develop, leading to weight loss, atypical fat distribution (Larson et al., 2006), and later serious multiorgan damage, including eye, kidney, peripheral nervous system, and brain damage (Biessels and Gispen, 2005). The slowly progressing alterations in cerebral function and structure that occur in diabetes are often referred to as diabetic encephalopathy. The clinical manifestations of diabetic encephalopathy include changes in cognitive function, such as moderate impairment of verbal memory and mental speed (Awad et al., 2004). These changes are very similar to those observed in HIV-associated dementia; in fact, the incidence of dementia doubles in elderly individuals who are diabetic and HIV positive (Valcour et al., 2004b, 2005).

In HIV-infected patients, particularly those with wasting syndrome or in children with failure to thrive (FTT), reduced levels of serum IGF-I have been observed (Laue et al., 1990; Jain et al., 1998). As IGF-I is a principal mediator of the action of human growth hormone, its role in anabolic effects has prompted studies on IGF-I levels in HIV-infected patients and the use of both IGF-I and growth hormone in the treatment of cachectic patients (Frost et al., 1996; Mynarcik et al., 1999, 2000; Lo et al., 2001). Although some improvements in body mass have been noted, results of some of these studies suggest partial resistance to growth hormone and IGF-I therapies in the setting of HIV wasting syndrome (Jain et al., 1998). Therefore, decreased levels of IGF-I in the CNS or alternatively development of insulin resistance may compromise neuronal survival during HIV infection, especially when HIVE develops.

To emphasize the protective effects IGF-IR signaling responses in neurons, we have devised PC12 cells that, in addition to their endogenous rat IGF-IR, over-express human IGF-IR cDNA (PC12/GR15; Ying Wang et al., 2003). In these cells, IGF-I stimulation triggers both PI-3K-Akt and Ras-Raf-MAP kinase signaling pathways, which are both strongly antiapoptotic (Gluckman et al., 1992; D'Mello et al., 1993; Baserga, 1995; Baserga et al., 1997a,b; Reiss et al., 1998; Adams et al., 2000; Gualco et al., 2009a). Although general antiapoptotic events after activation of the IGF-IR are well documented, its action against accumulation of intracellular ROS requires further explanation.

Despite mounting evidence showing that IGF-I accelerates aging and that ROS accumulation may be involved in this process (Sonntag et al., 1999; Holzenberger et al., 2003; Papaconstantinou, 2009), there are also reports indicating that IGF-I should improve cell survival. This is mainly because of its multiple antiapoptotic signals (Baserga et al.,

1997a; Peruzzi et al., 1999), the role of IGF-IR in protecting fetal brain tissue during development (Gualco et al., 2009a,b), and the supportive role of IGF-I in maintaining growth and survival of oli-godenrocyte progenitors (Arsenijevic et al., 2001; Hsieh et al., 2004). In addition to the antiapoptotic action of IGF-IR, IGF-I treatment can also counteract ROS accumulation in HG-treated mesanglial cells (Kang et al., 2003b; Yang et al., 2005), and HG-induced accumulation of intracellular ROS was partially inhibited by IGFI in PC12 neuron-like cells and in rat cortical neurons (this paper; Figs. 1, 3). Although we still do not know how IGF-I inhibits ROS accumulation, the effects of IGF-I on the signaling cross-talk between the pro-ROS protein p66Shc and the potentially anti-ROS protein FOXO3a (Nemoto and Finkel, 2002; Chintapalli et al., 2007; Guo et al., 2009; Husain et al., 2009) may help us to understand how the balance between prosurvival (IGF-I) and antisurvival (ROS and TNFα) factors affects FOXO3a function and controls the fate of neurons in brain tissue chronically affected by diabetes and/or inflammation.

Acknowledgments

Contract grant sponsor: NIH; Contract grant number: 2PO1 NS043980/project 2 (to K.R., S.A.); Contract grant number: RO1CA095518 (to K.R.); Contract grant number: RO1MH079751 (to F.P.); Contract grant number: PO1NS043980/Neuropathology Core (to L.D.V., S.A.).

REFERENCES

Adams TE, Epa VC, Garrett TP, Ward CW. Structure and function of the type 1 insulin-like growth factor receptor. Cell Mol Life Sci. 2000; 57:1050–1093. [PubMed: 10961344]

Aprea S, Del Valle L, Mameli G, Sawaya BE, Khalili K, Peruzzi F. Tubulin-mediated binding of human immunodeficiency virus-1 Tat to the cytoskeleton causes proteasomal-dependent degradation of microtubule-associated protein 2 and neuronal damage. J Neurosci. 2006; 26:4054–4062. [PubMed: 16611822]

Arsenijevic Y, Weiss S, Schneider B, Aebischer P. Insulin-like growth factor-I is necessary for neural stem cell proliferation and demonstrates distinct actions of epidermal growth factor and fibroblast growth factor-2. J Neurosci. 2001; 21:7194–7202. [PubMed: 11549730]

Awad N, Gagnon M, Messier C. The relationship between impaired glucose tolerance, type 2 diabetes, and cognitive function. J Clin Exp Neuropsychol. 2004; 26:1044–1080. [PubMed: 15590460]

Barbaro G. HIV infection, highly active antiretroviral therapy and the cardiovascular system. Cardiovasc Res. 2003; 60:87–95. [PubMed: 14522410]

Barbaro G. Metabolic and cardiovascular complications of highly active antiretroviral therapy for HIV infection. Curr HIV Res. 2006; 4:79–85. [PubMed: 16454713]

Baserga R. The insulin-like growth factor I receptor: a key to tumor growth? Cancer Res. 1995; 55:249–252. [PubMed: 7812953]

Baserga R, Resnicoff M, D'Ambrosio C, Valentinis B. The role of the IGF-I receptor in apoptosis. Vitam Horm. 1997a; 53:65–98. [PubMed: 9197178]

Baserga R, Resnicoff M, Dews M. The IGF-I receptor and cancer. Endocrine. 1997b; 7:99–102. [PubMed: 9449042]

Baynes JW, Thorpe SR. Role of oxidative stress in diabetic complications: a new perspective on an old paradigm. Diabetes. 1999; 48:1–9. [PubMed: 9892215]

Biessels GJ, Gispen WH. The impact of diabetes on cognition: what can be learned from rodent models? Neurobiol Aging. 2005; 26(Suppl 1):36–41. [PubMed: 16223548]

Brunet A, Bonni A, Zigmond MJ, Lin MZ, Juo P, Hu LS, Anderson MJ, Arden KC, Blenis J, Greenberg ME. Akt promotes cell survival by phosphorylating and inhibiting a Forkhead transcription factor. Cell. 1999; 96:857–868. [PubMed: 10102273]

Burgering BM, Kops GJ. Cell cycle and death control: long live Forkheads. Trends Biochem Sci. 2002; 27:352–360. [PubMed: 12114024]

Burhans WC, Heintz NH. The cell cycle is a redox cycle: linking phase-specific targets to cell fate. Free Radic Biol Med. 2009; 47:1282–1293. [PubMed: 19486941]

Calza L, Manfredi R, Farneti B, Chiodo F. Incidence of hyperlipidaemia in a cohort of 212 HIV-infected patients receiving a protease inhibitor-based antiretroviral therapy. Int J Antimicrob Agents. 2003; 22:54–59. [PubMed: 12842328]

Carr A, Samaras K, Thorisdottir A, Kaufmann GR, Chisholm DJ, Cooper DA. Diagnosis, prediction, and natural course of HIV-1 protease-inhibitor-associated lipodystrophy, hyperlipidaemia, and diabetes mellitus: a cohort study. Lancet. 1999; 353:2093–2099. [PubMed: 10382692]

Chandra S, Mondal D, Agrawal KC. HIV-1 protease inhibitor induced oxidative stress suppresses glucose stimulated insulin release: protection with thymoquinone. Exp Biol Med. 2009; 234:442–453.

Chintapalli J, Yang S, Opawumi D, Goyal SR, Shamsuddin N, Malhotra A, Reiss K, Meggs LG. Inhibition of wild-type p66ShcA in mesangial cells prevents glycooxidant-dependent FOXO3a regulation and promotes the survival phenotype. Am J Physiol Renal Physiol. 2007; 292:F523–F530. [PubMed: 17077388]

Choi J, Oh S, Lee D, Oh HJ, Park JY, Lee SB, Lim DS. Mst1-FoxO signaling protects Naive T lymphocytes from cellular oxidative stress in mice. PLoS One. 2009; 4:e8011. [PubMed: 19956688]

Chong ZZ, Maiese K. Erythropoietin involves the phosphatidylinositol 3-kinase pathway, 14-3-3 protein and FOXO3a nuclear trafficking to preserve endothelial cell integrity. Br J Pharmacol. 2007; 150:839–850. [PubMed: 17339844]

D'Ambrosio C, Valentinis B, Prisco M, Reiss K, Rubini M, Baserga R. Protective effect of the insulin-like growth factor I receptor on apoptosis induced by okadaic acid. Cancer Res. 1997; 57:3264–3271. [PubMed: 9242459]

D'Mello SR, Galli C, Ciotti T, Calissano P. Induction of apoptosis in cerebellar granule neurons by low potassium: inhibition of death by insulin-like growth factor I and cAMP. Proc Natl Acad Sci U S A. 1993; 90:10989–10993. [PubMed: 8248201]

Dansen TB, Burgering BM. Unravelling the tumor-suppressive functions of FOXO proteins. Trends Cell Biol. 2008; 18:421–429. [PubMed: 18715783]

Davila D, Torres-Aleman I. Neuronal death by oxidative stress involves activation of FOXO3 through a two-arm pathway that activates stress kinases and attenuates insulin-like growth factor I signaling. Mol Biol Cell. 2008; 19:2014–2025. [PubMed: 18287535]

De Bruyne E, Bos TJ, Schuit F, Van Valckenborgh E, Menu E, Thorrez L, Atadja P, Jernberg-Wiklund H, Vanderkerken K. IGF-1 suppresses Bim expression in multiple myeloma via epigenetic and posttranslational mechanisms. Blood. 2010; 115:2430–2440. [PubMed: 20086250]

Del Valle L, Pina-Oviedo S. HIV disorders of the brain: pathology and pathogenesis. Front Biosci. 2006; 11:718–732. [PubMed: 16146764]

Domingos H, Cunha RV, Paniago AM, Martins DM, Elkhoury EB, Souza AS. Metabolic effects associated to the highly active antiretroviral therapy (HAART) in AIDS patients. Braz J Infect Dis. 2009; 13:130–136. [PubMed: 20140358]

Essaghir A, Dif N, Marbehant CY, Coffer PJ, Demoulin JB. The transcription of FOXO genes is stimulated by FOXO3 and repressed by growth factors. J Biol Chem. 2009; 284:10334–10342. [PubMed: 19244250]

Feingold KR, Krauss RM, Pang M, Doerrler W, Jensen P, Grunfeld C. The hypertriglyceridemia of acquired immunodeficiency syndrome is associated with an increased prevalence of low density lipoprotein subclass pattern. B. J Clin Endocrinol Metab. 1993; 76:1423–1427.

Frost RA, Fuhrer J, Steigbigel R, Mariuz P, Lang CH, Gelato MC. Wasting in the acquired immune deficiency syndrome is associated with multiple defects in the serum insulin-like growth factor system. Clin Endocrinol. 1996; 44:501–514.

Gilley J, Coffer PJ, Ham J. FOXO transcription factors directly activate bim gene expression and promote apoptosis in sympathetic neurons. J Cell Biol. 2003; 162:613–622. [PubMed: 12913110]

Gluckman P, Klempt N, Guan J, Mallard C, Sirimanne E, Dragunow M, Klempt M, Singh K, Williams C, Nikolics K. A role for IGF-1 in the rescue of CNS neurons following hypoxic- ischemic injury. Biochem Biophys Res Commun. 1992; 182:593–599. [PubMed: 1370886]

Grunfeld C, Kotler DP, Hamadeh R, Tierney A, Wang J, Pierson RN. Hypertriglyceridemia in the acquired immunodeficiency syndrome. Am J Med. 1989; 86:27–31. [PubMed: 2910092]

Gualco E, Urbanska K, Perez-Liz G, Sweet T, Peruzzi F, Reiss K, Del Valle L. IGF-IR dependent expression of Survivin is required for T-antigen mediated protection from apoptosis and proliferation of neural progenitors. Cell Growth Differ. 2009a (in press).

Gualco E, Wang JY, Del Valle L, Urbanska K, Peruzzi F, Khalili K, Amini S, Reiss K. IGF-IR in neuroprotection and brain tumors. Front Biosci. 2009b; 14:352–375.

Guo J, Gertsberg Z, Ozgen N, Steinberg SF. p66Shc Links alpha1-adrenergic receptors to a reactive oxygen species-dependent AKT-FOXO3A phosphorylation pathway in cardiomyocytes. Circ Res. 2009; 104:660–669. [PubMed: 19168439]

Hadigan C. Insulin resistance among HIV-infected patients: unraveling the mechanism. Clin Infect Dis. 2005; 41:1341–1342. [PubMed: 16206113]

Hadigan C. Diabetes, insulin resistance, and HIV. Curr Infect Dis Rep. 2006; 8:69–75. [PubMed: 16448603]

Hasegawa K, Wakino S, Yoshioka K, Tatematsu S, Hara Y, Minakuchi H, Washida N, Tokuyama H, Hayashi K, Itoh H. Sirt1 protects against oxidative stress-induced renal tubular cell apoptosis by the bidirectional regulation of catalase expression. Biochem Biophys Res Commun. 2008; 372:51–56. [PubMed: 18485895]

Hasty P, Campisi J, Hoeijmakers J, van Steeg H, Vijg J. Aging and genome maintenance: lessons from the mouse? Science. 2003; 299:1355–1359. [PubMed: 12610296]

Hertel J, Struthers H, Horj CB, Hruz PW. A structural basis for the acute effects of HIV protease inhibitors on GLUT4 intrinsic activity. J Biol Chem. 2004; 279:55147–55152. [PubMed: 15496402]

Hoffmann O, Zipp F, Weber JR. Tumour necrosis factor-related apoptosis-inducing ligand (TRAIL) in central nervous system inflammation. J Mol Med. 2009; 87:753–763. [PubMed: 19449143]

Holzenberger M, Dupont J, Ducos B, Leneuve P, Geloen A, Even PC, Cervera P, Le Bouc Y. IGF-1 receptor regulates lifespan and resistance to oxidative stress in mice. Nature. 2003; 421:182–187. [PubMed: 12483226]

Hsieh J, Aimone JB, Kaspar BK, Kuwabara T, Nakashima K, Gage FH. IGF-I instructs multipotent adult neural progenitor cells to become oligodendrocytes. J Cell Biol. 2004; 164:111–122. [PubMed: 14709544]

Hui DY. Effects of HIV protease inhibitor therapy on lipid metabolism. Prog Lipid Res. 2003; 42:81–92. [PubMed: 12547652]

Husain M, Meggs LG, Vashistha H, Simoes S, Griffiths KO, Kumar D, Mikulak J, Mathieson PW, Saleem MA, Del Valle L, Pina-Oviedo S, Wang JY, Seshan SV, Malhotra A, Reiss K, Singhal PC. Inhibition of p66ShcA longevity gene rescues podocytes from HIV-1-induced oxidative stress and apoptosis. J Biol Chem. 2009; 284:16648–16658. [PubMed: 19383602]

Jain S, Golde DW, Bailey R, Geffner ME. Insulin-like growth factor-I resistance. Endocr Rev. 1998; 19:625–646. [PubMed: 9793761]

Kang BP, Frencher S, Reddy V, Kessler A, Malhotra A, Meggs LG. High glucose promotes mesangial cell apoptosis by oxidant-dependent mechanism. Am J Physiol Renal Physiol. 2003a; 284:F455–F466. [PubMed: 12419773]

Kang BP, Urbonas A, Baddoo A, Baskin S, Malhotra A, Meggs LG. IGF-1 inhibits the mitochondrial apoptosis program in mesangial cells exposed to high glucose. Am J Physiol Renal Physiol. 2003b; 285:F1013–F1024. [PubMed: 12876069]

Koeppe J, Kosmiski L. Apparent resolution of type 2 diabetes mellitus after initiation of potent antiretroviral therapy in a man from Africa with HIV infection. Clin Infect Dis. 2006; 42:e79–e81. [PubMed: 16619143]

Kops GJ, Dansen TB, Polderman PE, Saarloos I, Wirtz KW, Coffer PJ, Huang TT, Bos JL, Medema RH, Burgering BM. Forkhead transcription factor FOXO3a protects quiescent cells from oxidative stress. Nature. 2002; 419:316–321. [PubMed: 12239572]

Krause JC, Toye MP, Fisher DJ, Stechenberg BW, Reiter EO, Allen HF. Metabolic abnormalities in human immunodeficiency virusinfected children: two-year follow-up. J Pediatr Endocrinol Metab. 2009; 22:345–351. [PubMed: 19554809]

Larson R, Capili B, Eckert-Norton M, Colagreco JP, Anastasi JK. Disorders of glucose metabolism in the context of human immunodeficiency virus infection. J Am Acad Nurse Pract. 2006; 18:92–103. [PubMed: 16499742]

Laue L, Pizzo PA, Butler K, Cutler GB Jr. Growth and neuroendocrine dysfunction in children with acquired immunodeficiency syndrome. J Pediatr. 1990; 117:541–545. [PubMed: 2170610]

Lee HY, Youn SW, Kim JY, Park KW, Hwang CI, Park WY, Oh BH, Park YB, Walsh K, Seo JS, Kim HS. FOXO3a turns the tumor necrosis factor receptor signaling towards apoptosis through reciprocal regulation of c-Jun N-terminal kinase and NF-kappaB. Arterioscler Thromb Vasc Biol. 2008; 28:112–120. [PubMed: 18032780]

Lees SJ, Childs TE, Booth FW. Age-dependent FOXO regulation of p27Kip1 expression via a conserved binding motif in rat muscle precursor cells. Am J Physiol Cell Physiol. 2008; 295:C1238–C1246. [PubMed: 18787071]

Liu JW, Chandra D, Rudd MD, Butler AP, Pallotta V, Brown D, Coffer PJ, Tang DG. Induction of prosurvival molecules by apoptotic stimuli: involvement of FOXO3a and ROS. Oncogene. 2005; 24:2020–2031. [PubMed: 15674333]

Lo JC, Mulligan K, Noor MA, Schwarz JM, Halvorsen RA, Grunfeld C, Schambelan M. The effects of recombinant human growth hormone on body composition and glucose metabolism in HIV-infected patients with fat accumulation. J Clin Endocrinol Metab. 2001; 86:3480–3487. [PubMed: 11502767]

Matheny RW Jr, Adamo ML. Role of Akt isoforms in IGF-I-mediated signaling and survival in myoblasts. Biochem Biophys Res Commun. 2009; 389:117–121. [PubMed: 19703413]

Mynarcik DC, Frost RA, Lang CH, DeCristofaro K, McNurlan MA, Garlick PJ, Steigbigel RT, Fuhrer J, Ahnn S, Gelato MC. Insulin-like growth factor system in patients with HIV infection: effect of exogenous growth hormone administration. J Acquir Immune Defic Syndr. 1999; 22:49–55. [PubMed: 10534146]

Mynarcik DC, McNurlan MA, Steigbigel RT, Fuhrer J, Gelato MC. Association of severe insulin resistance with both loss of limb fat and elevated serum tumor necrosis factor receptor levels in HIV lipodystrophy. J Acquir Immune Defic Syndr. 2000; 25:312–321. [PubMed: 11114831]

Nakamura T, Sakamoto K. Forkhead transcription factor FOXO subfamily is essential for reactive oxygen species-induced apoptosis. Mol Cell Endocrinol. 2008; 281:47–55. [PubMed: 18035477]

Nemoto S, Finkel T. Redox regulation of forkhead proteins through a p66shc-dependent signaling pathway. Science. 2002; 295:2450–2452. [PubMed: 11884717]

Nishikawa T, Edelstein D, Du XL, Yamagishi S, Matsumura T, Kaneda Y, Yorek MA, Beebe D, Nolan D. Metabolic complications associated with HIV protease inhibitor therapy. Drugs. 2003; 63:2555–2574. [PubMed: 14636077]

Oates PJ, Hammes HP, Giardino I, Brownlee M. Normalizing mitochondrial superoxide production blocks three pathways of hyperglycaemic damage. Nature. 2000; 404:787–790. [PubMed: 10783895]

Papaconstantinou J. Insulin/IGF-1 and ROS signaling pathway cross-talk in aging and longevity determination. Mol Cell Endocrinol. 2009; 299:89–100. [PubMed: 19103250]

Peruzzi F, Prisco M, Dews M, Salomoni P, Grassilli E, Romano G, Calabretta B, Baserga R. Multiple signaling pathways of the insulin-like growth factor 1 receptor in protection from apoptosis. Mol Cell Biol. 1999; 19:7203–7215. [PubMed: 10490655]

Rathbone CR, Booth FW, Lees SJ. FoxO3a preferentially induces p27Kip1 expression while impairing muscle precursor cell-cycle progression. Muscle Nerve. 2008; 37:84–89. [PubMed: 17894357]

Reiss K, Valentinis B, Tu X, Xu SQ, Baserga R. Molecular markers of IGF-I-mediated mitogenesis. Exp Cell Res. 1998; 242:361–372. [PubMed: 9665833]

Rosso R, Di Biagio A. Evaluation of insulin resistance in a cohort of HIV-infected youth. Curr Diabetes Rep. 2009; 9:260–261.

Ryan LA, Peng H, Erichsen DA, Huang Y, Persidsky Y, Zhou Y, Gendelman HE, Zheng J. TNF-related apoptosis-inducing ligand mediates human neuronal apoptosis: links to HIV-1-associated dementia. J Neuroimmunol. 2004; 148:127–139. [PubMed: 14975593]

Salehian B, Bilas J, Bazargan M, Abbasian M. Prevalence and incidence of diabetes in HIV-infected minority patients on protease inhibitors. J Natl Med Assoc. 2005; 97:1088–1092. [PubMed: 16173323]

Shor-Posner G, Basit A, Lu Y, Cabrejos C, Chang J, Fletcher M, Mantero-Atienza E, Baum MK. Hypocholesterolemia is associated with immune dysfunction in early human immunodeficiency virus-1 infection. Am J Med. 1993; 94:515–519. [PubMed: 7605397]

Sonntag WE, Lynch CD, Cefalu WT, Ingram RL, Bennett SA, Thornton PL, Khan AS. Pleiotropic effects of growth hormone and insulin-like growth factor (IGF)-1 on biological aging: inferences from moderate caloric-restricted animals. J Gerontol A Biol Sci Med Sci. 1999; 54:B521–B538. [PubMed: 10647962]

Susztak K, Raff AC, Schiffer M, Bottinger EP. Glucose-induced reactive oxygen species cause apoptosis of podocytes and podocyte depletion at the onset of diabetic nephropathy. Diabetes. 2006; 55:225–233. [PubMed: 16380497]

Ting HH, Timimi FK, Boles KS, Creager SJ, Ganz P, Creager MA. Vitamin C improves endothelium-dependent vasodilation in patients with noninsulin-dependent diabetes mellitus. J Clin Invest. 1996; 97:22–28. [PubMed: 8550838]

Troiano L, Ferraresi R, Lugli E, Nemes E, Roat E, Nasi M, Pinti M, Cossarizza A. Multiparametric analysis of cells with different mitochondrial membrane potential during apoptosis by polychromatic flow cytometry. Nat Protoc. 2007; 2:2719–2727. [PubMed: 18007607]

Trojanek J, Ho T, Del Valle L, Nowicki M, Wang JY, Lassak A, Peruzzi F, Khalili K, Skorski T, Reiss K. Role of the insulin-like growth factor I/insulin receptor substrate 1 axis in Rad51 trafficking and DNA repair by homologous recombination. Mol Cell Biol. 2003; 23:7510–7524. [PubMed: 14559999]

Valcour V, Paul R. HIV infection and dementia in older adults. Clin Infect Dis. 2006; 42:1449–1454. [PubMed: 16619159]

Valcour V, Shikuma C, Shiramizu B, Watters M, Poff P, Selnes O, Holck P, Grove J, Sacktor N. Higher frequency of dementia in older HIV-1 individuals: the Hawaii Aging with HIV-1 Cohort. Neurology. 2004a; 63:822–827. [PubMed: 15365130]

Valcour V, Shikuma C, Shiramizu B, Watters M, Poff P, Selnes OA, Grove J, Liu Y, Abdul-Majid KB, Gartner S, Sacktor N. Age apolipoprotein E4, and the risk of HIV dementia: the Hawaii Aging with HIV Cohort. J Neuroimmunol. 2004b; 157:197–202. [PubMed: 15579298]

Valcour VG, Shikuma CM, Shiramizu BT, Williams AE, Watters MR, Poff PW, Grove JS, Selnes OA, Sacktor NC. Diabetes, insulin resistance, and dementia among HIV-1-infected patients. J Acquir Immune Defic Syndr. 2005; 38:31–36. [PubMed: 15608521]

Valcour VG, Sacktor NC, Paul RH, Watters MR, Selnes OA, Shiramizu BT, Williams AE, Shikuma CM. Insulin resistance is associated with cognition among HIV-1-infected patients: the Hawaii Aging With HIV cohort. J Acquir Immune Defic Syndr. 2006; 43:405–410. [PubMed: 17099311]

Valentinis B, Reiss K, Baserga R. Insulin-like growth factor-I-mediated survival from anoikis: role of cell aggregation and focal adhesion kinase. J Cell Physiol. 1998; 176:648–657. [PubMed: 9699518]

Valentinis B, Morrione A, Peruzzi F, Prisco M, Reiss K, Baserga R. Anti-apoptotic signaling of the IGF-I receptor in fibroblasts following loss of matrix adhesion. Oncogene. 1999; 18:1827–1836. [PubMed: 10086337]

Vigano A, Brambilla P, Pattarino G, Stucchi S, Fasan S, Raimondi C, Cerini C, Giacomet V, Zuccotti GV, Bedogni G. Long-term evaluation of glucose homeostasis in a cohort of HAART-treated HIV-infected children: a longitudinal, observational cohort study. Clin Drug Invest. 2009; 29:101–109.

Walli R, Goebel FD, Demant T. Impaired glucose tolerance and protease inhibitors. Ann Intern Med. 1998; 129:837–838. [PubMed: 9841594]

Wang H, Joseph JA. Quantifying cellular oxidative stress by dichlorofluorescein assay using microplate reader. Free Radic Biol Med. 1999; 27:612–616. [PubMed: 10490282]

Wang JY, Grabacka M, Marcinkiewicz C, Staniszewska I, Peruzzi F, Khalili K, Amini S, Reiss K. Involvement of alpha1beta1 integrin in insulin-like growth factor-1-mediated protection of PC12

neuronal processes from tumor necrosis factor-alpha-induced injury. J Neurosci Res. 2006; 83:7–18. [PubMed: 16307448]

Wang JY, Gualco E, Peruzzi F, Sawaya BE, Passiatore G, Marcinkiewicz C, Staniszewska I, Ferrante P, Amini S, Khalili K, Reiss K. Interaction between serine phosphorylated IRS-1 and beta1-integrin affects the stability of neuronal processes. J Neurosci Res. 2007; 85:2360–2373. [PubMed: 17593555]

Xing HQ, Hayakawa H, Izumo K, Kubota R, Gelpi E, Budka H, Izumo S. In vivo expression of proinflammatory cytokines in HIV encephalitis: an analysis of 11 autopsy cases. Neuropathology. 2009; 29:433–442. [PubMed: 19170891]

Yang S, Chintapalli J, Sodagum L, Baskin S, Malhotra A, Reiss K, Meggs LG. Activated IGF-1R inhibits hyperglycemia-induced DNA damage and promotes DNA repair by homologous recombination. Am J Physiol Renal Physiol. 2005; 289:F1144–F1152. [PubMed: 15956778]

Ying Wang J, Peruzzi F, Lassak A, Del Valle L, Radhakrishnan S, Rappaport J, Khalili K, Amini S, Reiss K. Neuroprotective effects of IGF-I against TNFalpha-induced neuronal damage in HIV-associated dementia. Virology. 2003; 305:66–76. [PubMed: 12504542]

Zheng WH, Kar S, Quirion R. Insulin-like growth factor-1-induced phosphorylation of the forkhead family transcription factor FKHRL1 is mediated by Akt kinase in PC12 cells. J Biol Chem. 2000; 275:39152–39158. [PubMed: 10995739]

Zheng X, Zhang Y, Chen YQ, Castranova V, Shi X, Chen F. Inhibition of NF-kappaB stabilizes gadd45alpha mRNA. Biochem Biophys Res Commun. 2005; 329:95–99. [PubMed: 15721278]

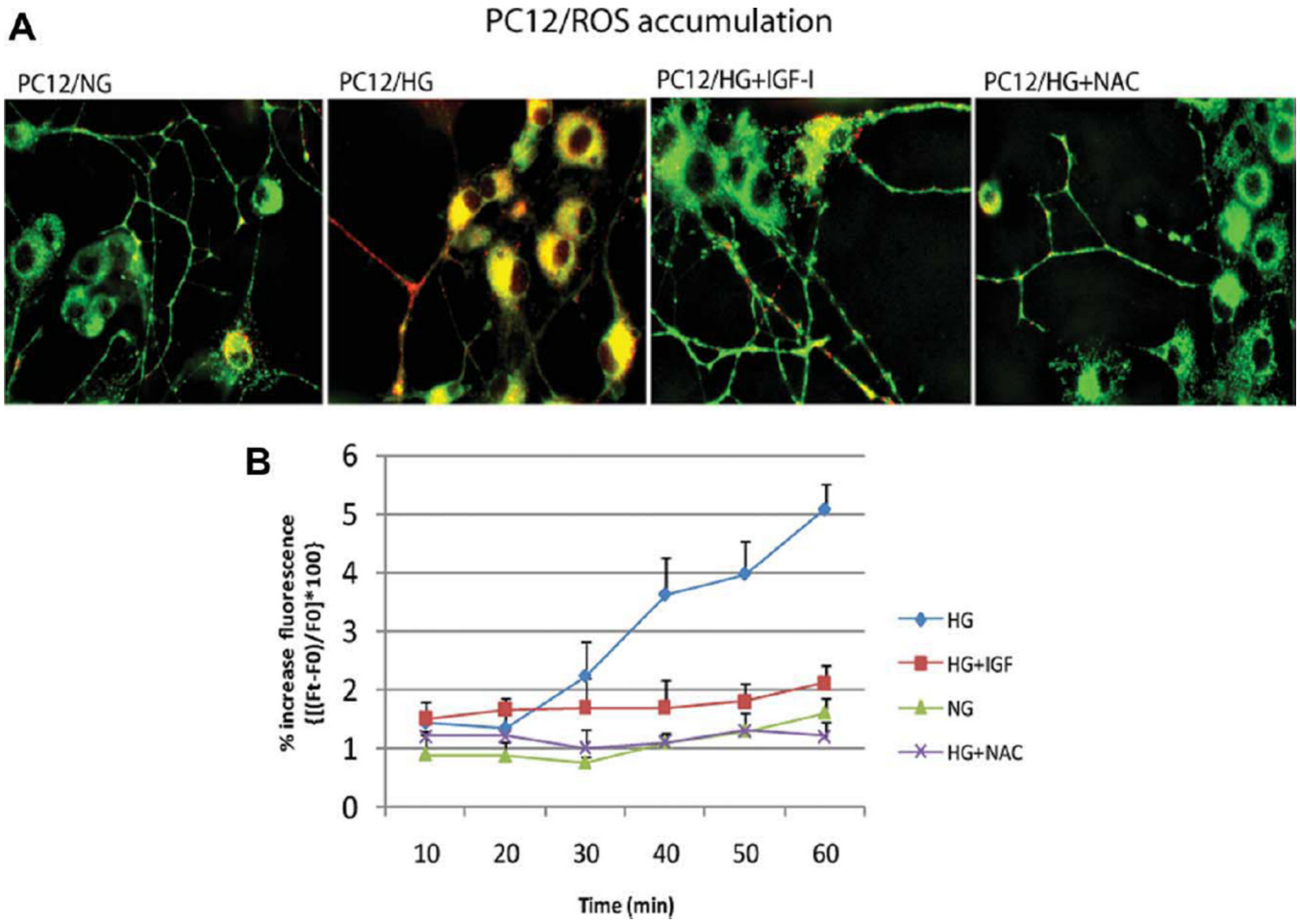

Fig. 1.

Effects of high glucose (HG) on ROS accumulation in differentiated neurons. **A**: Microscopic detection of ROS in differentiated PC12 neuron-like cells. Viable cells were loaded with 1 μM oxidant-sensitive dye redox sensor red CC-1 and with 50 nM mitochondria-specific dye Mito Tracker green FM. Representative fluorescent images show mitochondrial (yellow fluorescence) and cytosolic (red fluorescence) ROS accumulation in PC12 cells following 16 hr of incubation in the presence of 25 mM glucose (HG). Much lower levels of ROS accumulation were observed in control cultures in which differentiated neurons were kept in normal glucose concentration (NG; 5 mM) or in HG in the presence of the ROS scavenger N-acetylcysteine (NAC). Interestingly, HG-mediated ROS accumulation was effectively prevented by the IGF-I treatment (50 ng/ml). **B**: Quantitative analysis of ROS accumulation. Differentiated PC12 cells cultured in 24-well plates were loaded with 10 μM fluorescent dye 2′,7′-dichlorofluorescein diacetate (DCFDA). The measurements of ROS were performed in a CytoFluor multiwell plate reader. The kinetics of ROS accumulation were evaluated every 10 min for a period of 1 hr following the initial 16-hr cell preincubation in HG. Note the lack of ROS accumulation in neuronal cultures incubated under NG and in HG when the medium was additionally supplemented with NAC or IGF-I. Each experimental point was calculated from three separated experiments, and each experiment was repeated four times (n = 12). [Color figure can be viewed in the online issue, which is available at wileyonlinelibrary.com.]

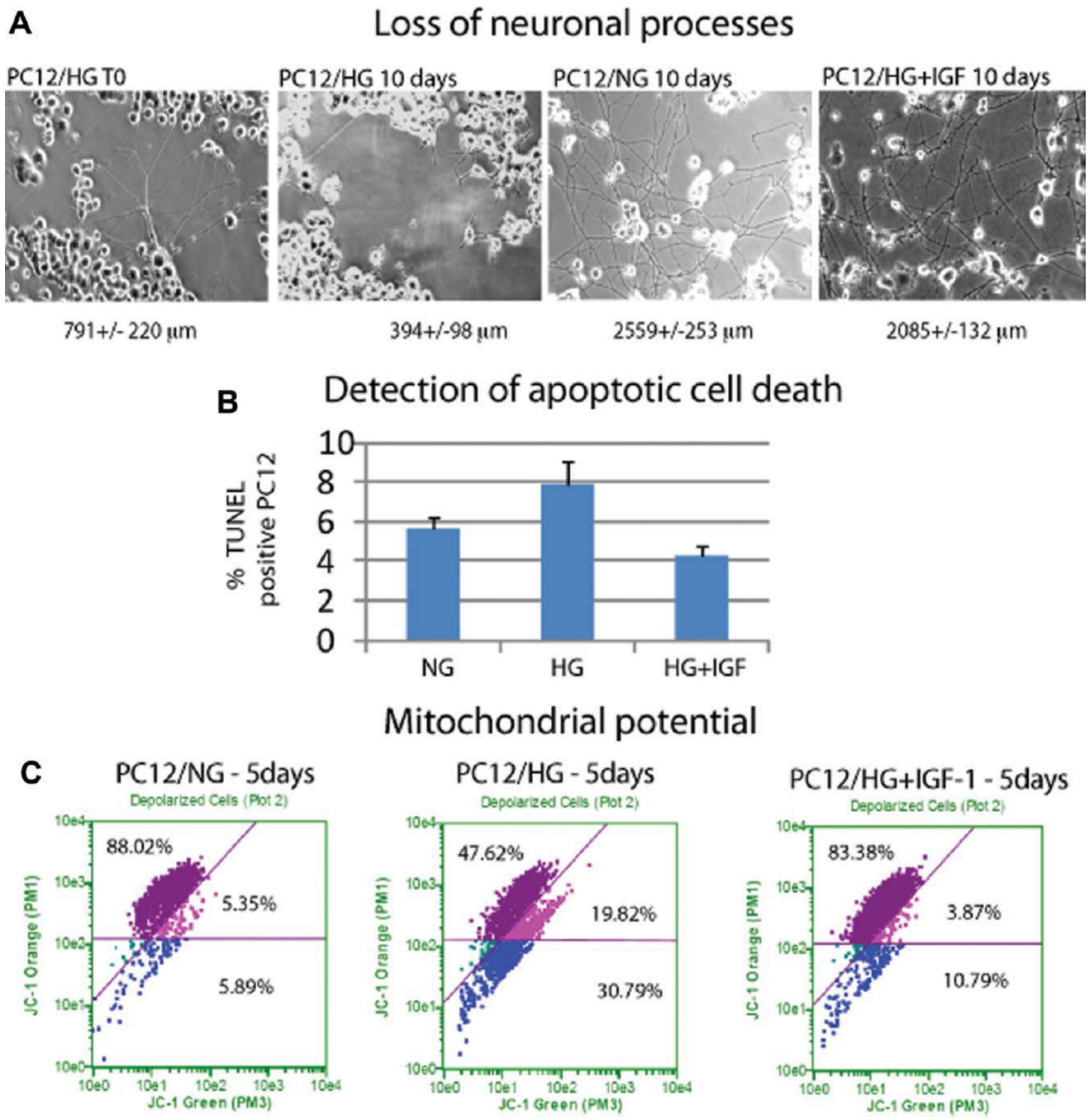

Fig. 2.

Effect of HG and IGF-I on the stability of neuronal processes. **A**: Phase-contrast images of differentiated cultures of PC12/GR15 neuron-like cells at day 0 (PC12/HG T0) and at day 10 following cell incubation in HG (PC12/HG; 10 days) and NG (PC12/NG; 10 days). In the presence IGF-I (HG + IGF-I; 10 days) HG-treated PC12 cultures do not show any apparent signs of the retraction of neuronal processes. The numbers below the images indicate average total lengths of neuronal processes per image with standard deviation (n = 10). **B**: Parallel PC12/GR15 cultures were used for the evaluation of apoptotic death by utilizing TUNEL assays. Note that the levels of apoptotic death detected in differentiated PC12/GR15

cells exposed to HG are not much different from the background apoptosis detected in NG. **C**: Loss of mitochondrial inner transmembrane potential ($\Delta\psi m$) was evaluated by a cationic dye, JC-1, which gives either green or orange fluorescence depending on mitochondrial membrane depolarization. Differentiated PC12/GR15 cells were cultured in NG, HG, and HG + IGF-I. After 5 days of incubation, the cells were harvested by trypsinization, loaded with JC-1 for 30 min, and immediately analyzed by Guava EastCyte flow cytometer using Mito-Potential software. The graph represents an example of $\Delta\psi m$ selected from three independent experiments performed in triplicate, all showing similar changes in $\Delta\psi m$. The cell population in the first quarter represents healthy unaffected cells (predominant orange); the second quarter contains cells with compromised mitochondrial potential (orange and green), and the third quarter contains cells with lost mitochondrial potential (predominant green; likely undergoing cell death). [Color figure can be viewed in the online issue, which is available at wileyonlinelibrary.com.]

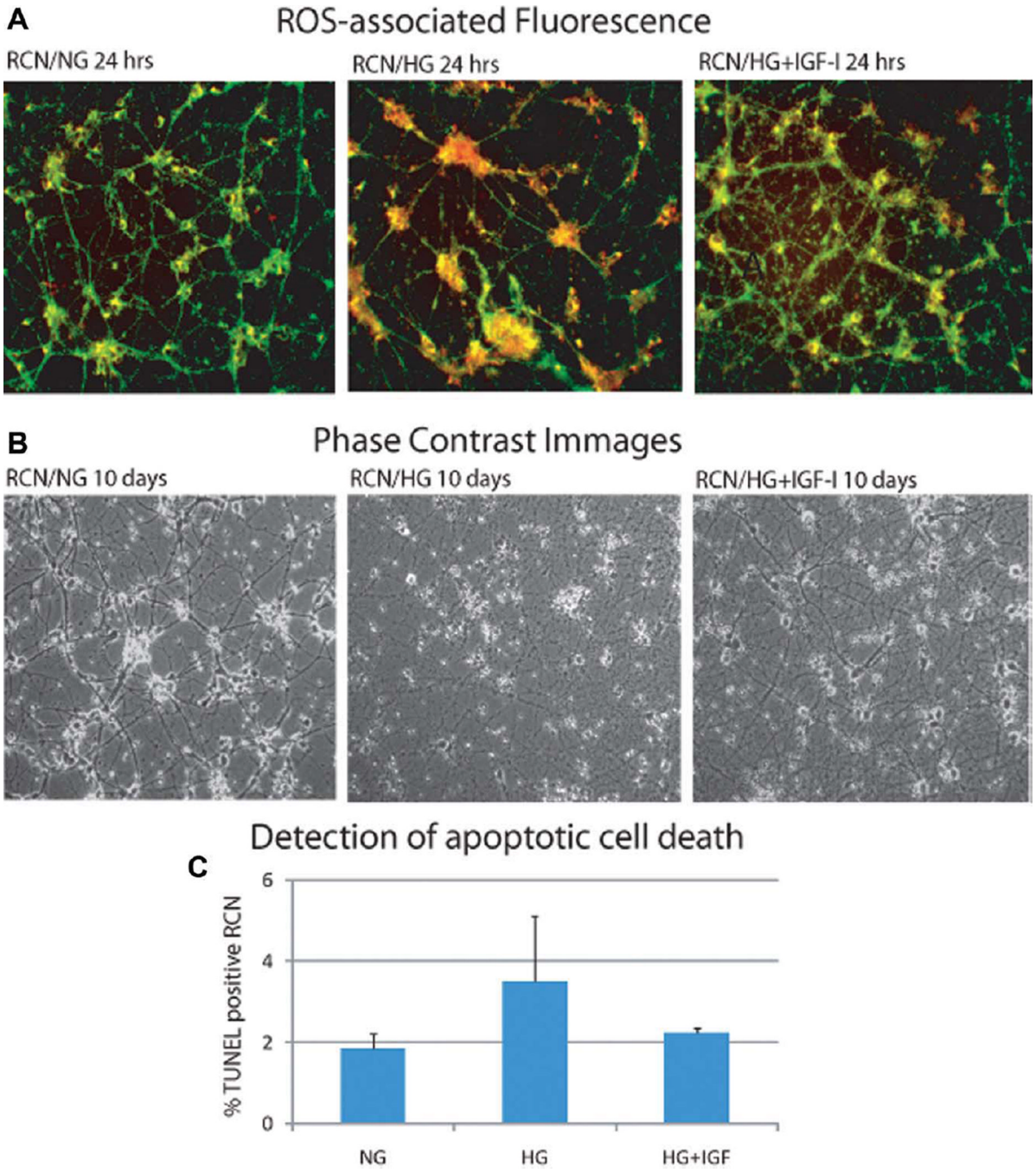

Fig. 3.

Microscopic detection of ROS in differentiated rat cortical neurons (RCN). Primary cultures of differentiated fetal rat cortical neurons were exposed to NG, HG, and HG + IGF-I conditions. **A**: After 24 hr of preincubation, viable cells were loaded with 1 μM oxidant-sensitive dye redox sensor red CC-1 and with 50 nM of mitochondria-specific dye MitoTracker green FM. Representative fluorescent images show mitochondrial (yellow fluorescence) and cytosolic (red fluorescence) ROS accumulation in cortical neurons cultured in the presence of HG. Note that cells cultured either in NG or in HG + IGF-I are characterized by predominantly green mitochondrial fluorescence. **B**: Phase-contrast images

of differentiated cultures of rat cortical neurons at day 10 following cell incubation in normal glucose (RCN/NG 10 days) and in high glucose (RCN/HG, 10 days). In the presence of 50 nM IGF-I, HG cultures of RCN do not show any apparent signs of the loss of neuronal processes (RCN/HG + IGF-I, 10 days). **C**: Parallel cultures of RCN were used for the evaluation of apoptotic death by TUNEL assay. Note that average levels of apoptotic death in RCN cultured in HG are only slightly higher (not different statistically) than the levels of apoptosis detected in NG. [Color figure can be viewed in the online issue, which is available at wileyonlinelibrary.com.]

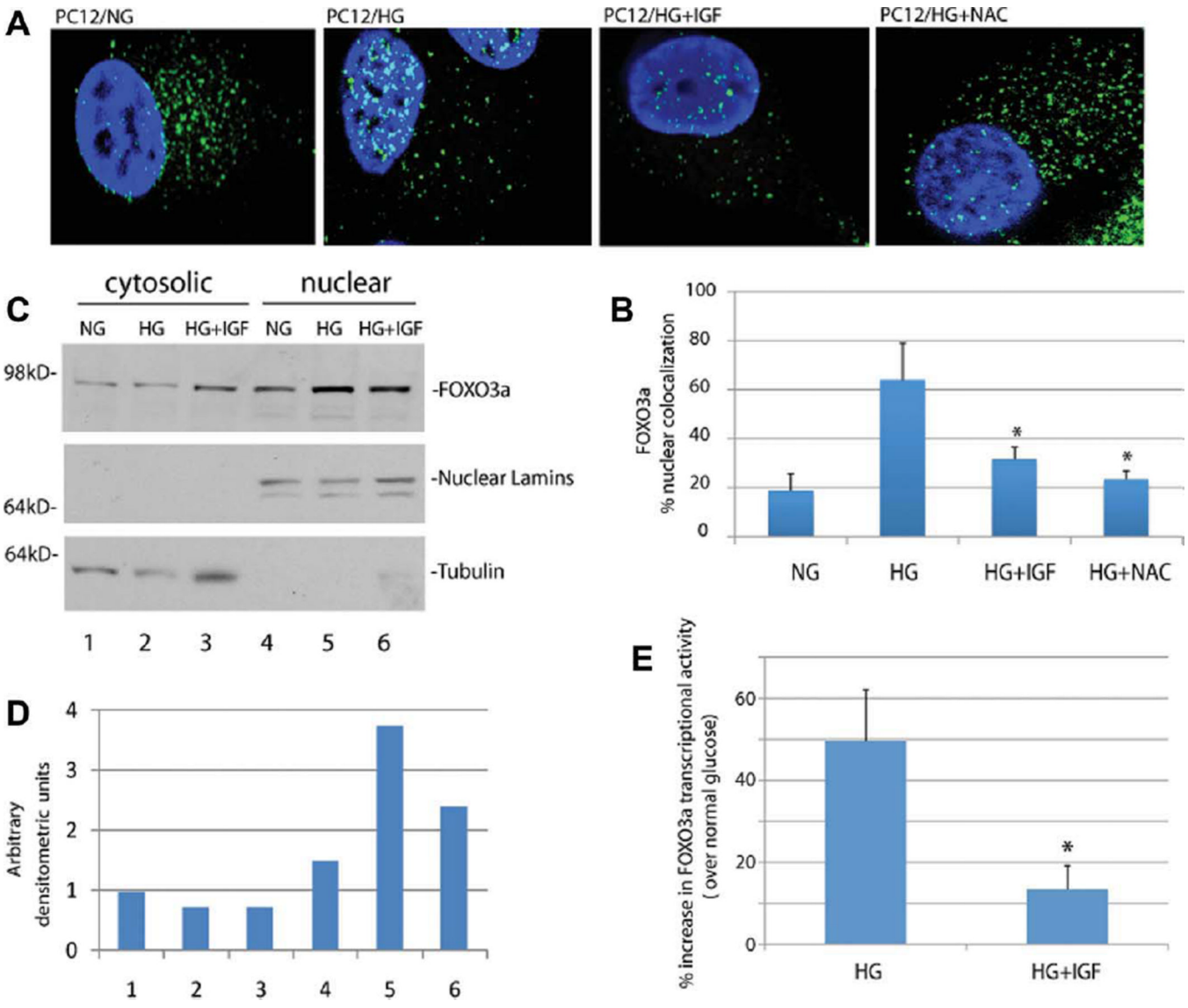

Fig. 4.

Effects of HG on subcellular localization and transcriptional activity of FOXO3a. Differentiated PC12/GR15 cells were cultures in the presence of NG, HG, HG + IGF-I, and HG + NAC. **A**: FOXO3a was detected by anti-FOXO3a rabbit polyclonal antibody (green fluorescence). DAPI staining was utilized to indicate the position of the nuclei (blue fluorescence). Fluorescent images were processed by utilizing inverted fluorescent microscope equipped with motorized z-axis and deconvolution software (SlideBook 4.1). Note that predominant cytosolic FOXO3a was detected in PC12/GR15 cells cultured under NG. Incubation of the cells in HG for 16 hr resulted in nuclear translocation of FOXO3a. The amount of nuclear FOXO3a decreased significantly when HG-treated cultures were supplemented either with IGF-I (HG + IGF-I) or the ROS scavenger N-acetylcysteine (NAC; HG + NAC). **B**: Quantification of the nuclear presence of FOXO3a [colocalization between FOXO3a immunolabeling (green fluorescence) and DAPI nuclear staining (blue fluorescence)] was performed by utilizing an inverted fluorescent microscope equipped with motorized z-axis and the Mask operation procedure included in the deconvolution software (SlideBook 4.1). **C**: Western blot analysis and fractionation of cellular compartments were

performed to provide an additional evaluation of changes in FOXO3a subcellular localization. Nuclear and cytosolic protein fractions were extracted from differentiated PC12/GR15 cells incubated in NG, HG, or HG + IGF-I, and the resulting blots were probed with anti-FOXO3a rabbit polyclonal antibody. **D**: Densitometry of the FOXO3a bands depicted in C was performed by utilizing EZQuant-Gel 2.17 software. Cytosolic FOXO3a was normalized by the corresponding α-tubulin bands, and nuclear FOXO3a was normalized by corresponding bands for nuclear lamins. **E**: Detection of FOXO3a transcriptional activity. PC12 cells were transfected with firefly-*Renilla* and FHRE-luciferase plasmid DNAs (ratio 1/3) by utilizing Lipofectamine 2000. The activation of FOXO3a-responsive elements (FHRE) was evaluated by a dual-firefly/*Renilla* luciferase reporter system (Promega). Note that IGF-I treatment decreased significantly HG-induced FOXO3a transcriptional activity. Data are presented as mean ± SD calculated from two experiments performed in triplicate (n = 6). [Color figure can be viewed in the online issue, which is available at wileyonlinelibrary.com.]

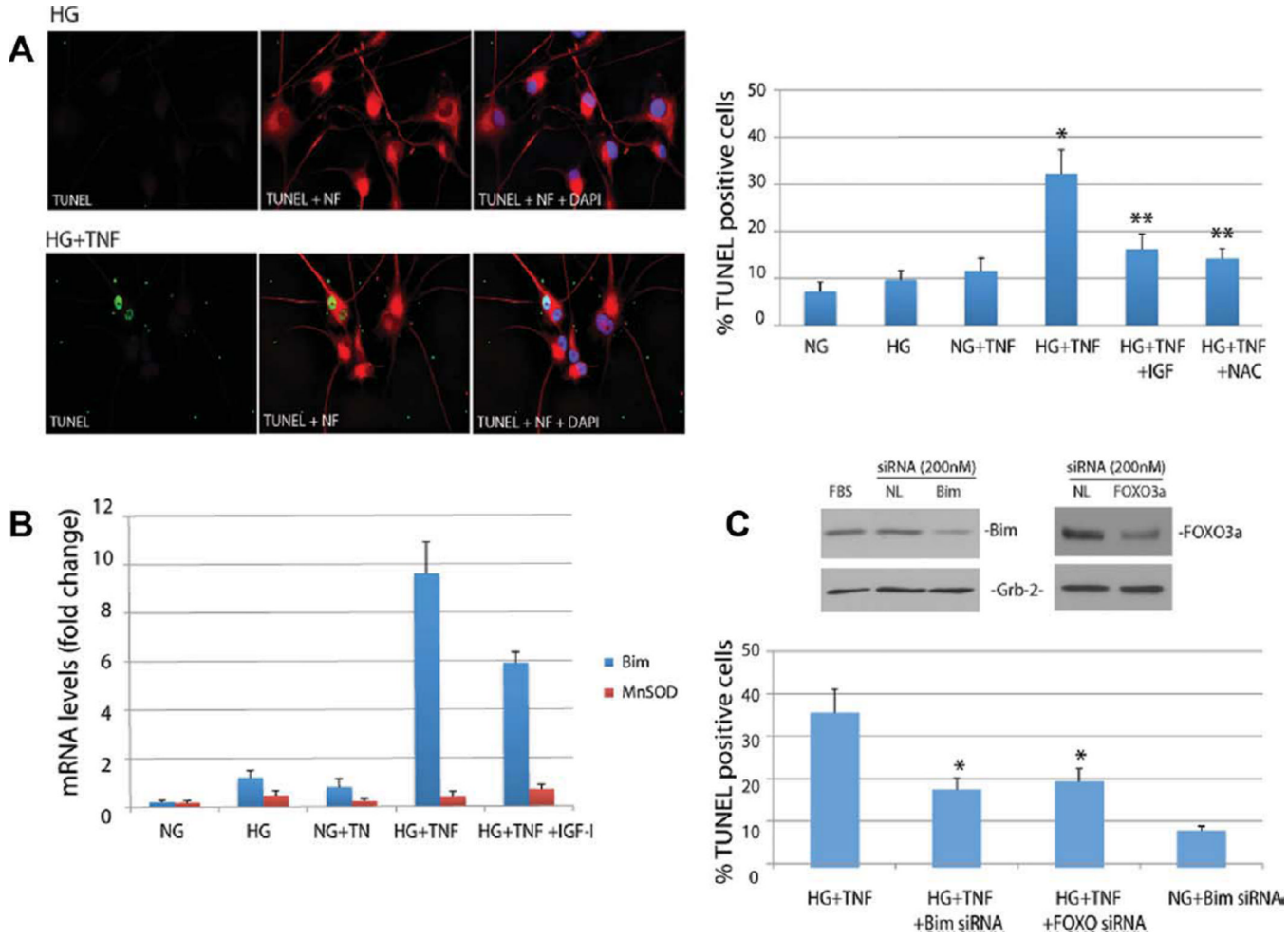

Fig. 5.

Combined action of HG and TNFα triggers FOXO3a-dependent Bim expression and activates neuronal apoptosis. Differentiated PC12/GR15 cells were cultured in the presence of NG, HG, HG + TNFα, or HG + TNFα + IGF-I. We have also used a potent ROS scavenger, N-acetylcysteine (NAC), to counteract HG-induced ROS accumulation. **A**: Example of neuronal apoptosis detected by the TUNEL assay following 5 days of incubation of differentiated PC12/GR15 cells with HG and HG + TNFα (100 ng/ml). Neuronal cells are visualized by immunolabeling with antineurofilament antibody (red fluorescence), TUNEL-positive nuclei show green fluorescence, and all nuclei are labeled with DAPI (blue fluorescence). Original magnification ×20. Histogram in A: Quantification of neuronal apoptosis in culture conditions described above. The data are presented as average percentage of TUNEL-positive cells with standard deviation. For each condition, 500 cells were counted in randomly selected microscopic fields in duplicate and the experiment was repeated three times (n = 6). *Significantly different from NG, HG, and NG + TNF; **significantly different from HG + TNF; $P = 0.05$. **B**: mRNA levels for two FOXO3adependent genes; Mn-dependent superoxide dismutase (MnSOD) and proapoptotic Bim, were evaluated by real-time RT-PCR. The data are presented as an average -fold increase of mRNA levels over mRNA levels detected in control conditions (NG) with standard deviation. *Significantly different from HG; $P = 0.05$. **C**: Effects of Bim and FOXO3a inhibition on HG− + TNFα-induced neuronal apoptosis. Differentiated PC12/GR15 cells were exposed to 200 nM smart pool siRNAs against rat Bim and FOXO3a

mRNAs for 72 hr. The percentage of apoptotic cells was evaluated by TUNEL assay. Data are presented as mean ± SD. *Statistically different from HG + TNF. **Inset**: Western blot analysis demonstrating Bim and FOXO3a protein levels in untreated cells (FBS), in cells exposed to irrelevant siRNA against nuclear lamins (NL), and in cells treated with siRNAs against Bim and FOXO3a. Grb-2 was used as an internal loading control. [Color figure can be viewed in the online issue, which is available at wileyonlinelibrary.com.]

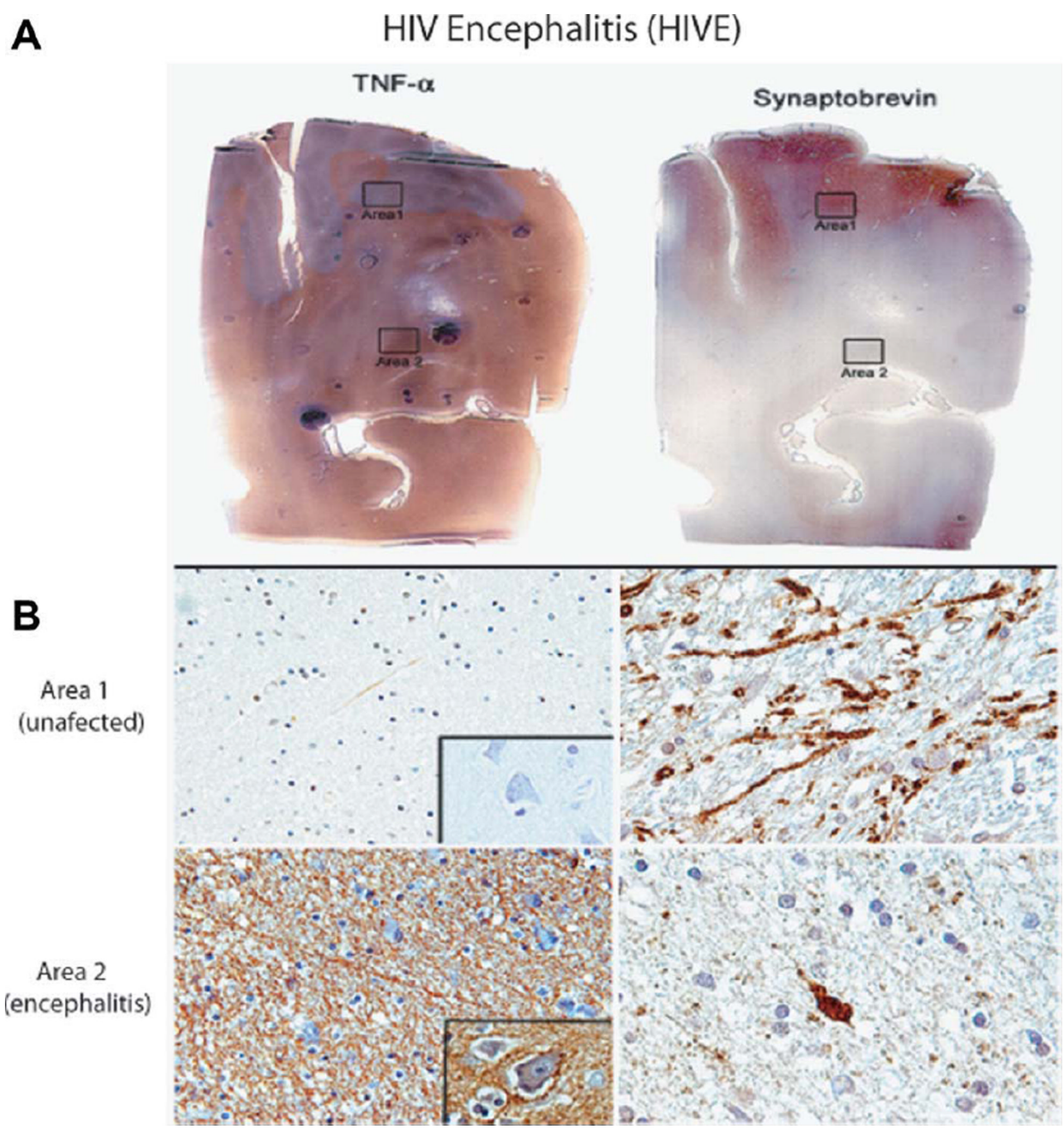

Fig. 6.

A,B: Immunohistochemical evaluation of TNFα accumulation in HIVE clinical samples. Consecutive sections from a case of HIVE immunolabeled for TNFα and synaptobrevin demonstrate the overall distribution pattern of these two proteins. In a nonaffected area (area 1), low levels of TNFα correlate with high levels of synaptobrevin. In contrast, in areas of severe inflammation (area 2), levels of TNFα are much higher, and synaptobrevin labeled neuronal processes are less apparent. Higher magnification images from areas 1 and 2 corroborate these findings. TNFα is practically undetectable in area 1, but its expression is strongly elevated in area 2. Synaptobrevin antibody labels well-preserved axons in area 1. In contrast, the area of a strong inflammation (area 2) is characterized by many fewer neuronal

processes and by other signs of neuronal damage, including an example of a retracted axon. [Color figure can be viewed in the online issue, which is available at wileyonlinelibrary.com.]

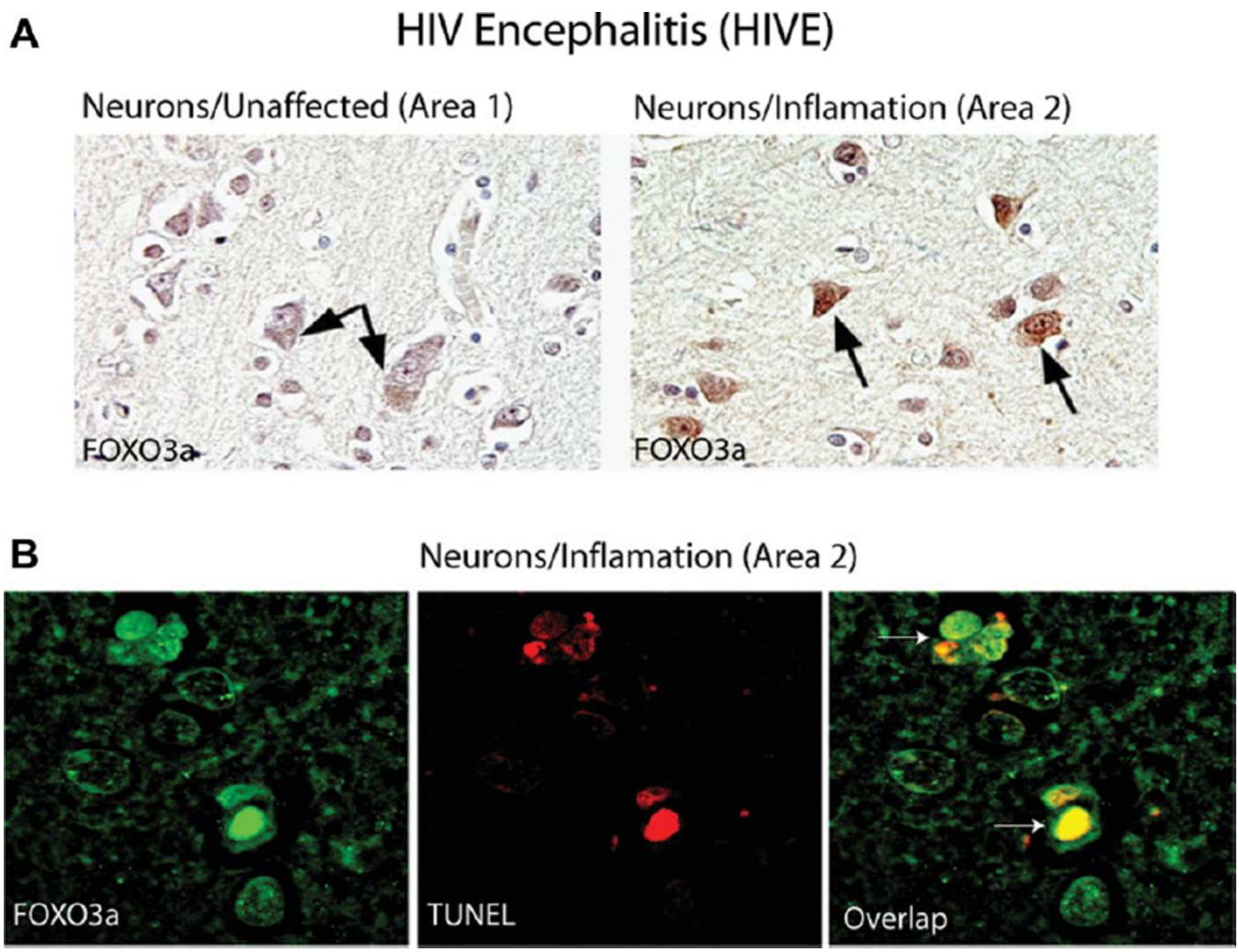

Fig. 7.

Detection of nuclear FOXO3a in apoptotic neurons from HIVE clinical samples. **A**: Immunohistochemical detection of FOXO3a in HIVE clinical samples was carried out with anti-FOXO3a rabbit polyclonal antibody (Cell Signaling). Neuronal cells from the control, unaffected (area 1 in Fig. 6) and inflammation-affected areas (area 2 in Fig. 6) of the brain (arrows) were evaluated. **B**: Dual-color immunofluorescence was performed to evaluate how subcellular localization of FOXO3a correlates with neuronal apoptosis evaluated by TUNEL. Rabbit anti-FOXO3a antibody was labeled with rhodamine-conjugated anti-rabbit IgG, and TUNEL-positive nuclei (arrows) were detected by FITC-based fluorescent labeling. The images were visualized with an inverted Nicon Eclipse TE300 microscope equipped with a Retiga 1300 camera, motorized z-axis, and deconvolution software (SlideBook 4.1). [Color figure can be viewed in the online issue, which is available at wileyonlinelibrary.com.]